Opto-Electronics Review

journal homepage: https://journals.pan.pl/opelre

Investigations of free electrons in doped silicon crystals derived from Fourier transformed infrared measurements and *ab initio* calculations

Bohdan Andriyevsky[1*], Leszek Bychto[1], Aleksy Patryn[1], Ulrich Schade[2], Ljiljana Puskar[2], Alexander Veber[2,3], Nikolay Abrosimov[4], Andrii I. Kashuba[5]

[1] Faculty of Electronics and Computer Sciences, Koszalin University of Technology, ul. Śniadeckich 2, 75-453 Koszalin, Poland
[2] Institute for Electronic Structure Dynamics, Helmholtz-Zentrum Berlin für Materialien und Energie GmbH, Albert-Einstein-Strasse 15, 12489 Berlin, Germany
[3] Department of Chemistry, Humboldt-Universität zu Berlin, Brook-Taylor-Strasse 2, 12489 Berlin, Germany
[4] Leibniz-Institut für Kristallzüchtung (IKZ), Max-Born-Strasse 2, 12489 Berlin, Germany
[5] Department of General Physics, Lviv Polytechnic National University, 12 Stepan Bandera St., 79013 Lviv, Ukraine

Article info

Article history:
Received 05 Sep. 2024
Received in revised form 07 Dec. 2024
Accepted 12 Dec. 2024
Available on-line 27 Jan. 2025

Keywords:
semiconductors;
doped silicon crystals;
far-infrared reflection spectra;
free electrons;
electron momentum scattering time;
effective mass of electron.

Abstract

The reflection spectra of *n*- and *p*-type silicon crystals doped with phosphorus and boron were measured for the free carrier concentrations of $1.1 \cdot 10^{15}$ cm^{-3} – $1.2 \cdot 10^{20}$ cm^{-3} in the far- and mid-infrared range between 20–3000 cm^{-1} using synchrotron radiation and Fourier transformed infrared technique. Transmittance spectra could be measured for lower sample carrier concentrations from the range studied. The measured reflection spectra were fitted by using the Drude relation and the parameters of free electron conductivity (electron effective mass m^* and momentum scattering time τ) were obtained for the *n*- and *p*-type-doped silicon. Additionally, the calculations of the band electronic structure and the electric conductivity σ of the crystals were performed in the framework of the density functional theory for different carrier concentrations and temperatures. The study main findings are (1) the substantial decrease of the momentum scattering time τ and (2) the clear increase of the electron effective mass m^* with an increase of the carrier concentrations N_c for both *n*- and *p*-type-doped silicon crystals.

1. Introduction

Doping plays a key role in all electronic devices, as all basic parameters of such devices are affected by dopant distributions. Doping refers to introducing impurity atoms in a controlled way to define the electrical properties in semiconductor materials (usually III and V group species). The donors and acceptors modify the electron and hole concentration from 10^{13} to 10^{21} cm^{-3}. The carrier concentration can also be spatially distributed to create *pn*-junctions and produce built-in electric fields. Most semiconductor devices use impurities (dopants) as a crucial ingredient to modify the electronic and optical properties, as well as the device structure [1].

Doping of semiconductors allows the manipulation of their electrical conductivity by exploiting the doping properties of the chemical elements in the main crystal matrix. By introducing a limited number of doping elements into the nominal crystal matrix, the conductivity of semiconductors can be significantly increased. The main challenges in this field are (1) ensuring the ability to control electrical conductivity by controlling the bandgap E_g and (2) ensuring the maximum mobility of free carriers (electrons or holes) [2]. Doping is critical to semiconductor devices, from transistors to thermoelectric energy converters. The interaction between electrons and impurities plays a key role in the transport of carriers. It turns out that high mobility of charge carriers can be achieved by properly selecting dopant elements to obtain high mobility in electronic, photonic, and energy conversion applications [3]. The *n*- and *p*-doped silicon

*Corresponding author at: bohdan.andriyevskyy@tu.koszalin.pl

https://doi.org/10.24425/opelre.2025.153756
1896-3757/ Association of Polish Electrical Engineers (SEP) and Polish Academic of Sciences (PAS). Published by PAS

crystals are widely used to fabricate different opto-electronic devices. That is why deepening the knowledge of their electronic structure is of interest. The commonly used substitutional doping of different elements, such as carbon, chalcogens, and phosphorus, induces various effects on silicon crystal structural, electronic, and optical properties [4–7].

It is known that the character of the temperature dependence of the electric conductivity (metal-like or semiconductor-like) of an extrinsic semiconductor depends on the concentration of residual carriers. A metal-like character occurs for relatively high carrier concentrations, while a semiconductor-like type is observed for relatively low carrier concentrations. This substantiates an approach in which the residual carriers may be divided into two parts: (1) the quasi-free and (2) the weakly bonded carriers. The quasi-free carriers are responsible for the metal-like electric conductivity, while the weakly bonded carriers correspond to the semiconductor-like one. The binding energy (eigenfrequency) of the quasi-free carriers is taken to be close to zero ($\omega_{01} = 0$), whereas the bonded ones may be characterised by one non-zero binding energy ($\omega_{02} \neq 0$). In this case, the Drude-Lorentz model of the frequency dependence of dielectric permittivity $\varepsilon(\omega)$ for electrons in a doped semiconductor may be presented in the following form:

$$\varepsilon(\omega) = \varepsilon_\infty - \frac{\omega_{p1}^2}{\omega^2 + i\gamma_1\omega} + \frac{\omega_{p2}^2}{\omega_{02}^2 - \omega^2 - i\gamma_2\omega}, \qquad (1)$$

where ε_∞ is the high-frequency dielectric permittivity, ω_{p1} and ω_{p2} are the plasma frequencies, ω_{02} is the eigenfrequency of the bonded electrons/holes, and γ_1 and γ_2 are the damping coefficients [8].

Investigations of the optical reflection and transmittance spectra of the pure and doped silicon crystals and associated properties of the quasi-free carriers (electrons and holes) are widely presented in the literature. Among these studies, systematic investigations of the carrier momentum scattering times/damping coefficients and the electron effective mass in the relatively wide range of free carrier concentrations, $10^{15} - 10^{21}$ cm^{-1}, are not numerous. This is partly caused by a relatively small intensity of the frequently used globar light sources in the far-infrared range of $\lambda > 15$ μm. In the present study, the optical reflection and transmittance spectra were obtained using synchrotron radiation, which was much brighter in the far-infrared range of $\lambda > 15$ μm than the globar sources. This allowed for more valid reflection spectra of doped silicon crystals with relatively small carrier concentrations, $10^{15} - 10^{17}$ cm^{-1}.

The present study aims to deepen the knowledge of the electron/hole parameters of the doped silicon crystals in the relatively wide range of the free carrier concentrations, $10^{15} - 10^{21}$ cm^{-1}, by using the reflection/transmittance spectra in the far-infrared range of 20–3000 cm^{-1} obtained by using the synchrotron radiation. In this range, electrons are excited from doping states into conduction bands or from valence bands into acceptor states of the semiconductor. The results may be useful for practical applications of silicon crystals in microelectronics and optoelectronics.

Fourier transformed infrared (FTIR) spectroscopy is an accurate tool for precise measurements of the reflection and transmittance spectra. Assuming that reflection and transmittance of the sample obey the Fresnel's formula, several electron- and phonon-related values of the crystals under study can be obtained, which will be helpful in the following discussion and conclusions.

2. Experimental

The samples used in this study were $15 \times 15 \times 0.45$ mm^3. The thin plates were cut from the crystals mostly grown by the floating zone (FZ) technique (see Table 1 for details) and doped during the growth process using Phosphine for *n*-type and Diboran for *p*-type crystals. Some crystals under study with higher dopant concentrations were grown using the Czochralski technique (CZ). The surface orientation of all samples was (100). Four probe measurements at room temperature determined the samples resistivity.

The specular reflection of the doped silicon samples was taken at an incidence of 8° close to normal and with an opening angle of about 50 msr. A custom-built motorized reflection set-up for the spectrometer sample compartment was used and spectra were taken with a Vertex 70/v FTIR (Bruker) spectrometer in vacuum in the 20–3000 cm^{-1} frequency range. A highly intense and brilliant synchrotron radiation at the IRIS beamline [9] from the BESSY II electron storage ring of the Helmholtz-Zentrum Berlin (HZB) was applied as a source.

According to the Drude model of conductivity, the plasma frequency $\omega_p = \omega_{p1}$ (1) of the doped semiconductors depends strongly on the free-carrier (electron or holes) concentration N_c:

$$\omega_p^2 = \frac{N_c e^2}{\varepsilon_0 \varepsilon_\infty m^*}, \qquad (2)$$

where e is the electron charge, ε_0 is the dielectric constant, ε_∞ is the dielectric permittivity caused by the bonded electrons, m^* is the effective mass of the charge carriers in a semiconductor [10]. To see the quantitative values, Table 1 presents a numerical correspondence between the plasma frequency ω_p and the electron concentration N_c, according to (2), taking the free electron mass, m_0, as the effective mass, $m^* = m_0$. Plasma frequency for free-electron concentration below $1 \cdot 10^{15}$ cm^{-3} can reach the lower limit of the spectral range of the FTIR spectrometer and therefore is not experimentally accessible by the spectroscopic method applied in this study.

Table 1.
Plasma frequency ω_p *vs.* free electron concentration N_c calculated using (2) for $\varepsilon_\infty = 4.0$ and $m^* = 1.0\ m_0$ (m_0 is the free electron mass).

N_c /cm^{-3}	ω_p /cm^{-1}
$1 \cdot 10^{15}$	29.7
$1 \cdot 10^{16}$	94.1
$1 \cdot 10^{17}$	297
$1 \cdot 10^{18}$	941
$1 \cdot 10^{19}$	2976
$1 \cdot 10^{20}$	9410
$1 \cdot 10^{21}$	29758

By fitting the measured reflection spectrum $R(\omega)$ of the doped silicon crystals by (1) using the RefFIT software [11], the plasma frequency ω_{p1} and the dissipation coefficient γ_1 can be obtained. Afterward, the effective mass of electrons/holes m^* in the doped silicon crystals of the known carrier concentration N_c can be calculated from the fitted plasma frequency ω_p using (2) [8, 12].

2.1. *First-principle calculations*

Calculations of the electronic properties of the silicon crystals studied were performed in the framework of the density functional theory (DFT) using the Vienna *ab initio* simulation package (VASP) code [13–18]. Based on the generalized gradient approximation, the standard Perdew-Burke-Ernzerhof (PBE) exchange-and-correlation function [19] has been used.

To calculate silicon crystals electronic properties, a silicon crystal structure with cubic space group of symmetry *Fd-3m* (no. 227) was used.

The calculations were performed by VASP using projector-augmented wave PBE (PAW_PBE) pseudo-potentials, xc-functional PBE, and a cut-off energy of 500 eV for electron plane waves. One of the calculated values was the dielectric permittivity ε_∞ (dielectric permittivity caused by bonding electrons). A $3 \times 3 \times 3$ silicon supercell containing 216 atoms was used to calculate the dielectric permittivity ε_∞. The effective electron mass m^* and the corresponding electric conductivity of the *n*- and *p*-type silicon crystals were calculated within the constant relaxation time approximation using the AMSET software [20] developed based on VASP and BoltzTraP2 codes [13–18, 21]. The authors' calculations using the AMSET code used eight Si atoms in the unit cell ($1 \times 1 \times 1$) of a pure silicon crystal ($a = b = c = 5.44$ Å).

3. Results and discussion

The obtained experimental specular reflection spectra of doped silicon crystals are shown in Fig. 1. In these reflection spectra, the authors did not find the features that can be associated with excitations of bonded electrons or phonons. Therefore, the fitting of the experimental reflection spectra was performed using only free electrons, which means using only the first two members in the right part of (1):

$$\varepsilon(\omega) = \varepsilon_\infty - \frac{\omega_{p1}^2}{\omega^2 + i\gamma_1\omega}. \tag{3}$$

The corresponding fitted parameters are presented in Table 2.

In Table 2, the parameters of (2) and (3), ε_∞, ω_p, γ, and m^*, calculated by the RefFIT package based on the measured reflectance spectra $R(1/\lambda)$ of the samples, are dependent on the free carrier concentration N_c. A slight decrease of the dielectric constant ε_∞ observed with an increase of the free carrier concentration N_c (Table 2) may be caused by the screening of the light wave electric field by free electrons in the doped silicon crystals.

The experimental dependence of the square of plasma frequency ω_p^2 on the carrier concentration N_c reveals the nonlinear character, which can be fitted sufficiently well by the allometric function $y = a \cdot x^b$, with the coefficient b less than unity [$b = 0.877$, see Fig. 2(a)]. Considering (2) and the fitted coefficient $b < 1$, one can conclude that the monotonous increase of the effective mass m^* occurs at the increase of the carrier concentration N_c.

However, this fitting may not be sufficiently precise in all regions of the wide carrier concentration range of $10^{15} - 10^{21}$ cm^{-3}. To overcome this drawback, one can (1) use the double logarithmic scales for N_c and ω_p and (2) use a more complicated function containing more than two fitting parameters. Taking into account the latter comments, the fitting of the dependence $\omega_p(N_c)$ is realized in the double logarithmic scales using the logistic function containing four fitting parameters, $y = A_2 + (A_1 - A_2)/(1 + (x/x_0)^p)$ [Fig. 2(b)].

Having obtained the dependence $\omega_p(N_c)$ [Fig. 2(b)], the corresponding dependence of the effective electron masses m^* on the free carrier concentration N_c is calculated using (2) and presented in Table 2 and Fig. 3. In Fig. 3, the point corresponding to the electron carrier concentration $N_c = 5.6 \cdot 10^{17}$ cm^{-3} (Table 2) is omitted because of the substantial difference between the experimental and fitted

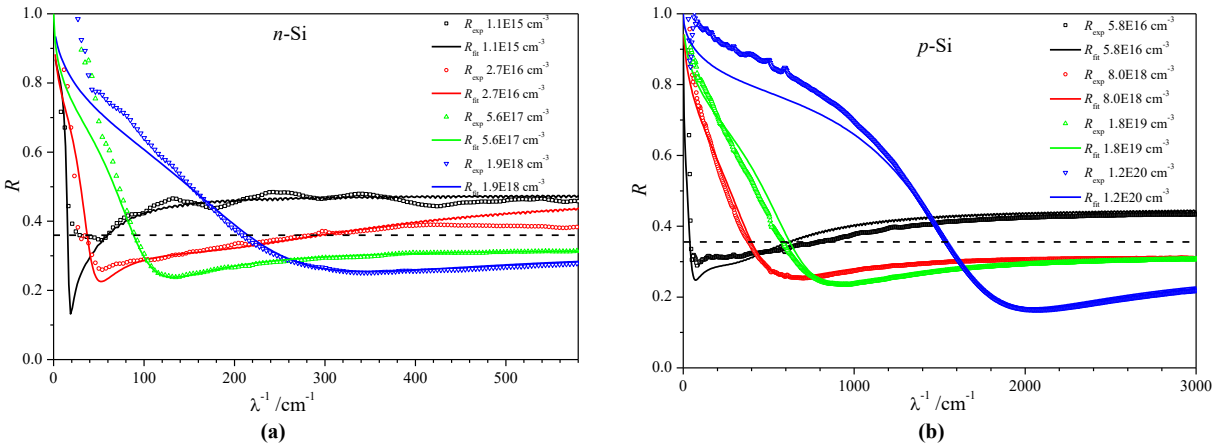

Fig. 1. Experimental (points) and fitted (lines) specular reflectance spectra of (a) *n*- and (b) *p*-doped $R(\lambda^{-1})$ silicon single crystals in the infrared range for different concentrations of N_c carriers, indicated by different colours. Horizontal dashed line indicates the reflection coefficient $R = [(n - 1/n + 1)]^2$ corresponding to the refractive index of a silicon single crystal caused by bonded electrons, $n = 3.6$ ($\varepsilon_\infty = 12.96$) for the wavelength $\lambda \approx 1$ μm [22].

Table 2.
Parameters derived from the fitting of the reflection spectra of *n*- and *p*-type-doped silicon single crystals of different carrier concentrations N_c using (2) and (3) and the RefFIT software [12]. The carrier momentum scattering time τ is proportional to the inverse damping coefficient γ in (1) and (3), $\tau = 1/(\gamma c)$, where c is the light velocity in vacuum.

Doping type/growth technique	N_c, cm^{-3}	ε_∞	ω_p, cm^{-1}	γ, cm^{-1}	τ, s	m^*, m_0
n / *FZ*	$1.1 \cdot 10^{15}$	12.96	61.7	4.52	$7.38 \cdot 10^{-12}$	0.079
n / *FZ*	$2.7 \cdot 10^{16}$	12.96	155	27.3	$1.22 \cdot 10^{-12}$	0.308
p / *FZ*	$5.8 \cdot 10^{16}$	12.96	192	58.0	$5.75 \cdot 10^{-13}$	0.429
n / *FZ*	$5.6 \cdot 10^{17}$	12.96	379	79.3	$4.20 \cdot 10^{-13}$	1.066
n / *FZ*	$1.9 \cdot 10^{18}$	12.96	952	246	$1.35 \cdot 10^{-13}$	0.574
p / *CZ*	$8 \cdot 10^{18}$	12.96	1754	459	$7.26 \cdot 10^{-14}$	0.712
p / *FZ*	$1.8 \cdot 10^{19}$	12.96	2644	543	$6.14 \cdot 10^{-14}$	0.705
p / *CZ*	$1.2 \cdot 10^{20}$	12.96	5984	775	$4.30 \cdot 10^{-14}$	0.918

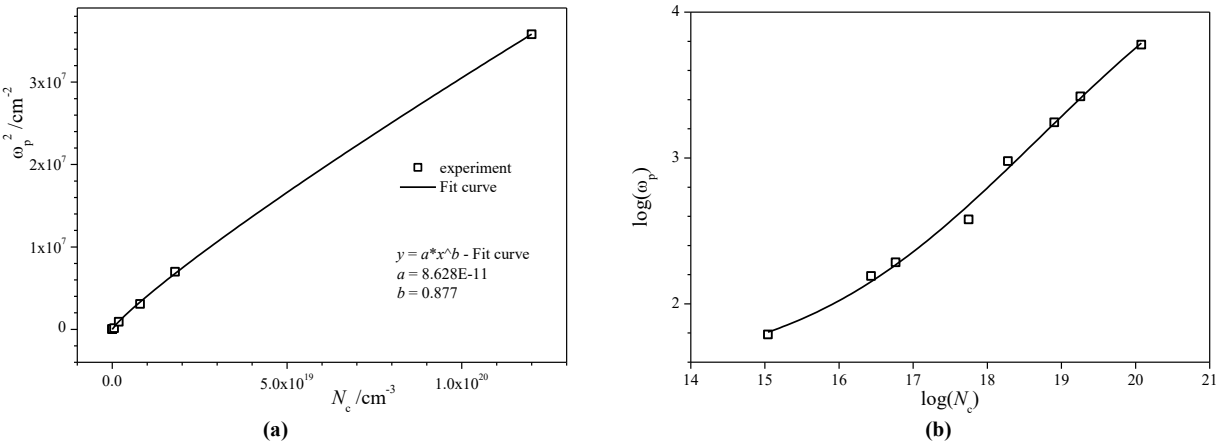

Fig. 2. (a) Dependences of the square of the plasma frequency ω_p^2 on the free carrier concentration N_c in the form of experimental points (Table 2) and a dashed curve (fitting the dependence of $\omega_p^2(N_c)$ to the power-like function $y = a \cdot x^b$) for the doped silicon crystals; (b) log-log dependence of the plasma frequency ω_p on the free carrier concentration N_c in the form of experimental points (Table 2) and a solid curve [fitting the dependence $\omega_p(N_c)$ to the logistic function $y = A_2 + (A_1 - A_2)/(1 + (x/x_0)^p]$ for the doped silicon crystals.

reflection spectra in Fig. 1(a). The latter circumstance could cause a large deviation of the effective mass m^* from the fitted linear dependence $m^*(\log(N_c))$ in Fig. 3. In the relatively wide range of the carrier concentration of 10^{15}–10^{20} cm^{-3}, the dependence $m^*(\log(N_c))$ in Fig. 3 is very close to linear. The second order polynomial fitting of the experimental dependence $m^*(\log(N_c))$ (points in Fig. 3),

$$m^* = -2.4172 + 0.1754 \log(N_c) - 5.5101 \cdot 10^{-4} (\log(N_c))^2 \quad (4)$$

allows the estimation of the effective electron mass m^* of the carriers in doped silicon crystals in a relatively wide range of carrier concentration of 10^{15}–10^{20} cm^{-3}.

The values of the effective electron mass of the doped silicon m^* in the carrier concentration range of $1 \cdot 10^{18} - 5 \cdot 10^{20}$ cm^{-3} obtained from the authors' experimental reflection spectra by using the Drude model (2), $m^* \approx 0.7\, m_0$ (Table 2 and Fig. 3), are larger than the reference data $m^* \approx 0.3\, m_0$ [23] for the corresponding concentration N_c. One of the possible reasons for this effective electron mass difference may be a different quality of the corresponding silicon samples, which can result in different values of the dielectric permittivity ε_∞. However, the latter point is not considered in some cases [24–26]. The authors have performed DFT calculations for

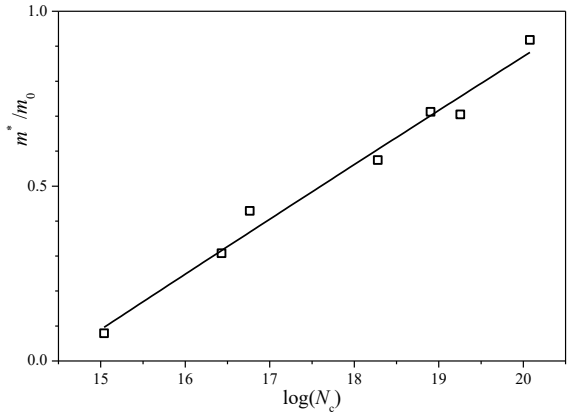

Fig. 3. Dependences of the effective electron mass m^* on the free carrier concentration N_c for the doped-silicon crystals obtained on the basis of the experimental far-infrared reflection spectra (squares – before fitting, solid line – after fitting).

pure silicon crystal and heavily phosphorus-doped silicon crystals ($N_c = 5 \cdot 10^{22}$ cm^{-3}) corresponding to one phosphorus and 215 silicon atoms in the supercell and they have found the increase of the dielectric permittivity ε_∞ from $\varepsilon_\infty = 11.46$ for the pure silicon crystal to $\varepsilon_\infty = 13.09$ for the phosphorus-

doped one. Consequently, the effective electron mass m^* calculated using (2) will be more negligible for a more significant value of the dielectric permittivity ε_∞. The increased dielectric permittivity ε_∞ in the phosphorus-doped silicon crystal is probably caused by donor energy states formed in the forbidden energy gap of the phosphorus-doped silicon crystal. This occurs because, according to the Kramers-Kronig relation, the input to the real part of the dielectric function ε_1 is inversely proportional to the energy difference between the ground and exited electron states. Similar DFT calculations of the heavily boron-doped silicon crystals ($N_c = 5 \cdot 10^{22}$ cm^{-3}) were performed and a decrease of the dielectric permittivity ε_∞ was detected ($\varepsilon_\infty = 10.38$) in comparison to the similar value for the pure silicon crystal, $\varepsilon_\infty = 11.46$.

In principle, another reason of errors leading to possible inaccuracies in estimating the effective electron mass m^* from the authors' far-infrared studies of doped silicon samples is an inaccurate calculation of the carrier concentration N_c based on the electric conductivity/resistivity measurements. Measurements of the electric conductivity/resistivity of the samples studied were performed by using the four-terminal sensing [27]. Afterward, the corresponding carrier concentrations N_c were calculated using the known formulae for the boron-doped and phosphorus-doped silicon crystals [28]. Thus, there are two sources of the possible inaccuracy in determining the carrier concentration N_c. One derives from the experimental measurements of the samples conductivity/resistivity and the other from the fixed formulae for calculating the carrier concentration based on the measured sample conductivity/resistivity [28].

To study the likely differences in the electron parameters of n- and p-doped silicon samples, the corresponding experimentally obtained dependences of the plasma frequencies on the carrier concentrations $\omega_p(N_c)$ are presented separately in Fig. 4(a). Here, a clear difference between two straight lines corresponding to the linear fitting of the logl-log $\omega_p(N_c)$ dependences for the n- and p-doped silicon samples is observed. Calculated dependences of the effective electron masses on the carrier concentration, $m^*_n(N_c)$ and $m^*_p(N_c)$ corresponding to these $p(N_c)$ dependences, are presented in Fig. 4(b). For the carrier concentration of $N_c < 2 \cdot 10^{17}$ cm^{-3}, the effective electron mass is smaller than the effective hole mass, $m^*_n < m^*_p$ [Fig. 4(b)]. The latter agrees with the known reference data for the conductivity effective mass in a silicon crystal, $m^*_n = 0.27$ and $m^*_p = 0.39$ [24]. For the carrier concentration of $N_c > 2 \cdot 10^{17}$ cm^{-3}, the opposite relation between the effective masses of $m^*_n > m^*_p$ takes place [Fig. 4(b)]. Such change of the sign of the effective mass difference $m^*_n - m^*_p$ with an increase of the carrier concentration, N_c, is the consequence of crossing the straight lines on the dependences $\log(\omega_p)$ on $\log(N_c)$ [Fig. 4(a)]. Taking into account that the DFT calculated dielectric permittivity of the heavily boron-doped silicon crystals, $\varepsilon_\infty = 10.38$, is smaller than the similar value for the pure silicon, $\varepsilon_\infty = 11.46$, the curve of the dependence $m^*_p(N_c)$ in Fig. 4(b) will be shifted a bit to the larger magnitudes of the effective mass, m^*_p. Thus, one may expect the relation of $m^*_n > m^*_p$ to take place for the carrier concentration a bit larger than the above-mentioned one $N_c > 2 \cdot 10^{17}$ cm^{-3}.

A clear increase of the damping coefficient γ with an increase in the free carrier concentration N_c observed (Table 2) is caused by a corresponding increase in the free electron-electron interaction/scattering. The observed inverse dependence of logarithm of the momentum scattering time $\log(\tau)$ ($\tau = 1/(\gamma c)$, where c is the light velocity on the logarithm of carrier concentration $\log(N_c)$ (Fig. 5), is a result of this interaction. Therefore, the free electron/hole momentum scattering time τ decreases by two orders of magnitude when the free carrier concentration N_c of the doped silicon crystals increases by four orders of magnitude (Fig. 5). For relatively low free carrier concentrations $N_c < 10^{17}$ cm^{-3}, the momentum scattering times of free electrons are a bit larger than the momentum scattering times of the holes (Fig. 5).

According to the theory of electron conductivity in metals, the direct proportionality between the conductivity σ and the carrier concentration N_c takes place if the momentum scattering time τ and effective mass m^* are constant:

$$\sigma = \frac{1}{\rho} = \frac{e^2 \tau N_c}{m^*}. \tag{5}$$

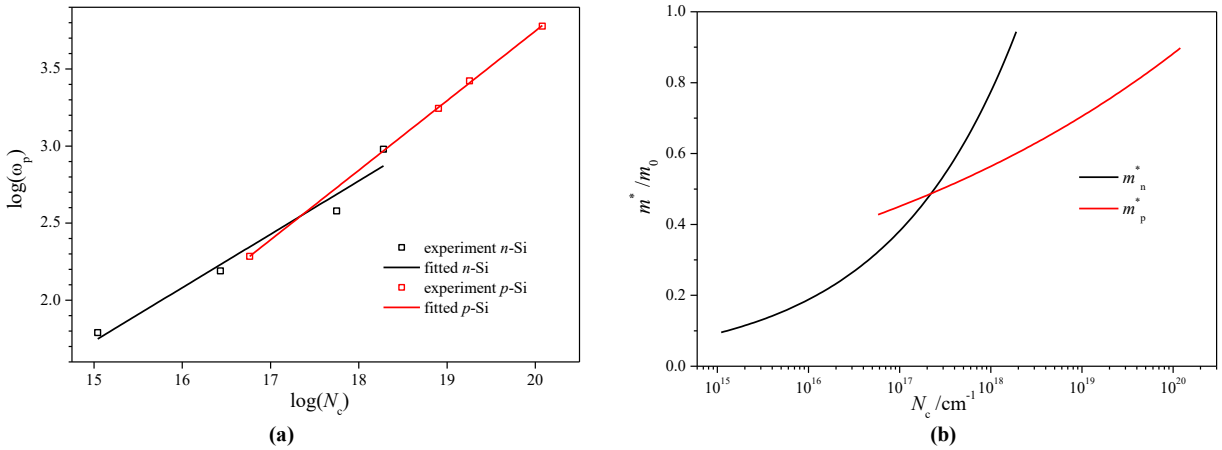

Fig. 4. (a) Log-log dependences of the plasma frequency ω_p on the free carrier concentration N_c in the form of experimental points (Table 2) and solid straight lines (linear fittings of the dependences $\omega_p(N_c)$ in the form of experimental points) for the doped-silicon crystals; (b) dependences of the effective electron/hole masses m^* on the logarithm of the carrier concentration N_c calculated using the fitted data in Fig. 4(a) and (2). Black and red colours correspond to the n- and p-type doping of silicon crystals.

This, however, is not realized because a clear nonlinearity of the dependences $\sigma_n(N_c^{(n)})$ and $\sigma_n(N_p^{(p)})$ is observed: the relation τ/m^* decreases with an increase of N_c [Fig. 6(a)]. This agrees with a relatively strong decrease of the momentum scattering time τ (Fig. 5) and a moderate increase of the effective mass m^* [Figs. 3(a), 4(b)]. Thus, the main reason for the observed nonlinearity of the dependences $\sigma_n(N_c^{(n)})$ and $\sigma_n(N_c^{(p)})$ is a decrease of the momentum scattering time τ with an increase in the carrier concentration N_c. The same conclusion can be derived from comparing the experimental and the theoretical dependences $\sigma(N_c)$ presented in log-log scales [Fig. 6(b)].

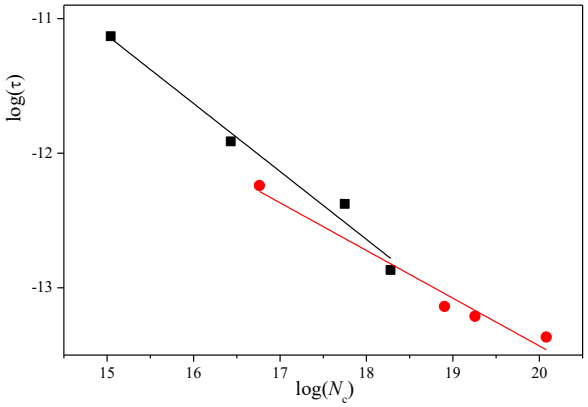

Fig. 5. Log-log dependences of the momentum scattering time τ on the free carrier concentration N_c in the form of experimental points (Table 2) and solid straight lines (linear fittings of the dependences $\log(\tau)$ on $\log(N_c)$ in the form of experimental points) for the doped silicon crystals.

The RefFIT fitted parameters of the doped silicon crystals presented in Table 2 were obtained using the model of a silicon plane parallel plate of a finite thickness (silicon crystals of a thickness of 0.45 mm) in vacuum. However, if one uses the model of an infinitely thick slab, the fitted parameter ε_∞ obtained for the carrier concentrations less than $N_c = 1 \cdot 10^{17}$ cm^{-3} is larger than those with concentrations of $N_c > 1 \cdot 10^{17}$ cm^{-3}. This is caused by an increase in the reflection coefficient R due to the partial transparency and back-side light reflection of the samples studied. The latter feature leads to an increase in the fitted parameter ε_∞. Figure 7 illustrates this effect. For the carrier concentration of $N_c = 5.6 \cdot 10^{17}$ cm^{-3} [Fig. 7(a)], the transmittance T of the sample is still relatively small and the light reflection is

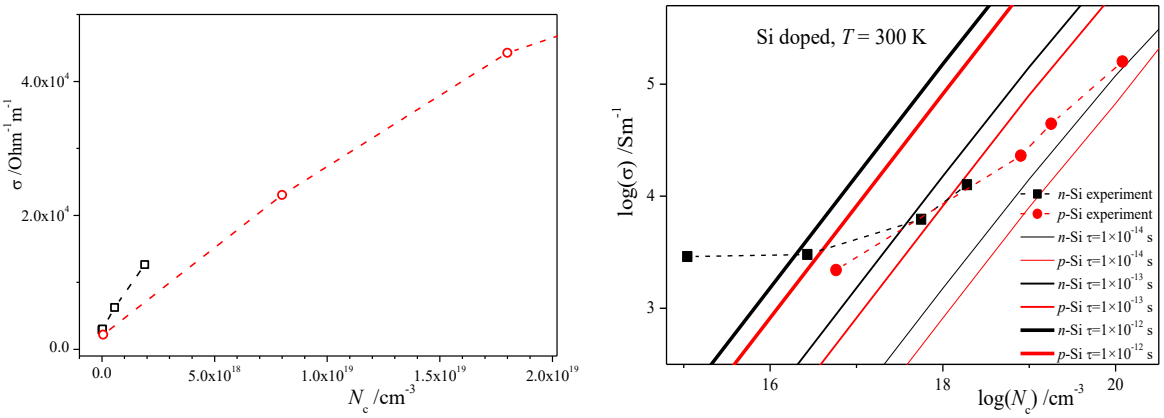

Fig. 6. (a) Dependences of the electric conductivity σ of silicon crystals on the free carrier concentration N_c corresponding to free electrons (black colour) and holes (red colour) obtained from the FTIR experiment; (b) dependences of the electric conductivity σ on the electron/hole concentration N_c in log-log scales for n- (black) and p-type (red) silicon crystals obtained from the FTIR experiment (points and dashed lines) and calculated using the AMSET code within the constant relaxation time approximation (solid lines).

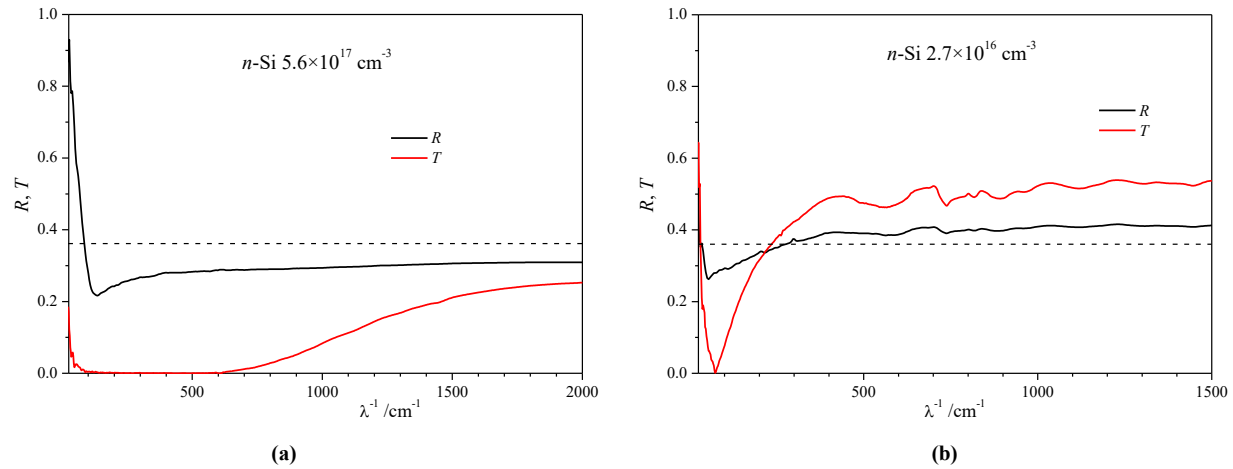

Fig. 7. Reflection and transmission spectra $R(\lambda^{-1})$ and $T(\lambda^{-1})$ of n-type-doped silicon single crystals for two carrier concentrations, (a) $N_c = 5.6 \cdot 10^{17}$ cm^{-3} and (b) $N_c = 2.7 \cdot 10^{16}$ cm^{-3}. Horizontal dashed line indicates the specular reflection coefficient R for the normal incidence and corresponding to the refractive index of a silicon single crystal $n = 3.6$ for the wavelength $\lambda \approx 1$ μm [22].

realized mainly from the front surface of the sample. This results in a case where the measured reflection coefficient [solid black curve in Fig. 7(a)] is smaller than the calculated one based of the refractive index of the silicon single crystal $n = 3.6$ for the wavelength $\lambda \approx 1$ μm [22] (dashed horizontal line), corresponding to the range of silicon transparency. For the carrier concentration of $N_c = 2.7 \cdot 10^{16}$ cm^{-3} [Fig. 7(b)], the transmittance T of the sample is relatively high and the light reflection is additionally realized from the back-side of the sample surface. This, in turn, results in the opposite case where the measured reflection coefficient [(solid black curve in Fig. 7(b)] becomes larger than the calculated one [dashed horizontal line in Fig. 7(b)].

4. Conclusions

By applying the Drude model of the frequency-dependent dielectric permittivity $\varepsilon(\omega)$ to the quasi-free electrons in the *n*- and *p*-doped silicon crystals of the carrier concentration in the range of 10^{15}–10^{20} cm^{-3}, the clear non-linear dependence of the square plasma frequency on the carrier concentration N_c is found. Analysis of this non-linearity reveals an increase in the electron effective mass m^* with an increase of the carrier concentration N_c. The dependence $m^*(\log(N_c))$ is close to the linear one in the relatively wide carrier concentration range of 10^{15}–10^{20} cm^{-3}. For the relatively low free carrier concentrations of $N_c < 10^{17}$ cm^{-3}, the electron effective masses m^*_n are smaller than the effective masses of the holes m^*_p.

For *n*- and *p*-doped silicon crystals studied, the free electron/hole momentum scattering time τ decreases more than two orders of magnitude when the free carrier concentration N_c increases in the range of 10^{15}–10^{20} cm^{-3}. For the relatively low free carrier concentrations of $N_c < 10^{17}$ cm^{-3}, the free electrons momentum scattering times are a bit larger than the momentum scattering times of the holes.

In the wide range of the carrier concentration N_c, the relation (5) between the electric conductivity σ and the free carrier concentration N_c in the doped silicon crystals is strongly nonlinear, which is revealed in a decrease of τ/m^* with an increase of N_c. This concentration decrease of τ/m^* is due to the simultaneous reduction in the momentum scattering time τ and the effective mass m^* increase. At the same time, the corresponding relative decrease of the momentum scattering time $|\Delta\tau/\tau|$ is approximately three times larger than the relative increase of the effective mass $|\Delta m^*/m^*|$. For the free carrier concentrations of $N_c < 2 \cdot 10^{18}$ cm^{-3}, the free electron conductivity σ_n is larger than the hole electric conductivity σ_p, that is in agreement with the corresponding relations for the momentum scattering times (τ_n, τ_p) and the effective masses (m^*_n, m^*_p).

Using the DFT calculations of the band electronic structure of doped silicon crystals, it was found that: (1) the heavily *n*-type doping ($N_c = 5 \cdot 10^{22}$ cm^{-3}), performed by the replacement of silicon atoms by the phosphorus atoms, leads to an increase in the dielectric permittivity ε_∞ of the crystal by about 13%; (2) the heavily *p*-type doping ($N_c = 5 \cdot 10^{22}$ cm^{-3}), performed by the replacement of silicon atoms with the boron atoms, leads to a decrease in the dielectric permittivity ε_∞ of the crystal by approximately 10%.

Authors' statement

Research concept and design, A.B., L.B., N.A. and A.P.; collection and/or assembly of data, A.B., L.B., U.S., L.P., A.I.K. and A.V.; data analysis and interpretation, A.B., L.B., A.V., U.S., L.P. and A.I.K.; writing the article, A.B., L.B., N.A., U.S. and A.V.; critical revision of the article, A.P. and A.V.; final approval of article, A.B. and L.B.

Acknowledgements

Experimental measurements were performed with infrared synchrotron radiation at the IRIS beamline of the electron storage ring BESSY II at the Helmholtz-Zentrum Berlin für Materialien und Energie in the framework of the BESSY proposal 232-12203-ST. Computer calculations were performed at ICM of Warsaw University, Poland (projects nos. g93-1636 and g96-1832) and WCSS of Wrocław University of Science and Technology, Poland (project no. 053).

References

[1] Tulsyan, G. Doping Profile Measurements in Silicon Using Terahertz Domain Spectroscopy (THz-TDS) Via Electrochemical Anodic Oxidation. (Rochester Institute of Technology, Rochester, N.Y., 2015).

[2] Yoo, H., Heo, K., Ansari, H. R. & Cho, S. Recent advances in electrical doping of 2D semiconductor materials: Methods, analyses, and applications. *Nanomaterials* **11**, 832 (2021). https://doi.org/10.3390/nano11040832

[3] Zhou, J. *et al*. Mobility enhancement in heavily doped semiconductors via electron cloaking. *Nat. Commun.* **13**, 2482 (2022). https://doi.org/10.1038/s41467-022-29958-2

[4] Lan, C.-W., Hsu, C. & Nakajima, K. 10-Multicrystalline Silicon Crystal Growth for Photovoltaic Applications. in *Handbook of Crystal Growth: Bulk Crystal Growth, Second Edition* (Ed. Rudolph, P.) II, 373–411 (Elsevier, 2015). https://doi.org/10.1016/B978-0-444-63303-3.00010-9

[5] Lan, C. W. *et al*. Engineering silicon crystals for photovoltaics. *CrystEngComm* **18**, 1474–1485 (2016). https://doi.org/10.1039/c5ce02343b

[6] Du, L., Yin, J., Zeng, W. & Yi, H. First-principles calculations to investigate electronic structures and optical properties of chalcogens-hyperdoped silicon. *Solid State Commun*. **342**, 114610 (2022). https://doi.org/10.1016/j.ssc.2021.114610

[7] Marri, I., Degoli, E. & Ossicini, S. First principle studies of B and P doped Si nanocrystals. *Phys. Status Solidi (A) Appl. Mater. Sci.* **215**, 1700414 (2018). https://doi.org/10.1002/pssa.201700414

[8] Yu, P. Y. & Cardona, M. *Fundamentals of Semiconductors*, *Physics and Materials Properties Fourth Ed.* (Springer, 2010). https://doi.org/10.1007/978-3-642-00710-1

[9] Schade, U., Ortolani, M. & Lee, J. Technical Report: THz experiments with coherent synchrotron radiation from BESSY II. *Synchrotron Radiat. News* **20**, 17–24 (2007). https://doi.org/10.1080/08940880701631351

[10] Sólyom, J. *Fundamentals of the Physics of Solids, Volume II: Electronic Properties*. (Springer-Verlag Berlin Heidelberg, 2009). https://doi.org/10.1007/978-3-540-85316-9

[11] Kuzmenko, A. B. Kramers-Kronig constrained variational analysis of optical data. *Rev. Sci. Instrum.* **76**, 083108 (2005). https://doi.org/10.1063/1.1979470

[12] Spitzer, W. G. & Fan, H. Y. Determination of optical constants and carrier effective mass of semiconductors. *Phys. Rev.* **106**, 882–890 (1957). https://doi.org/10.1103/PhysRev.106.882

[13] Kresse, G. & Hafner, J. *Ab initio* molecular dynamics for liquid metals. *Phys. Rev. B* **47**, 558–561 (1993). https://doi.org/10.1103/PhysRevB.47.558

[14] Kresse, G. & Hafner, J. *Ab initio* molecular-dynamics simulation of the liquid-metal-amorphous-semiconductor transition in germanium. *Phys. Rev. B* **49**, 14251–14269 (1994). https://doi.org/10.1103/PhysRevB.49.14251

[15] Kresse, G. & Furthmüller, J. Efficiency of ab-initio total energy calculations for metals and semiconductors using a plane-wave basis set. *Comput. Mater. Sci*. **6**, 15–50 (1996). https://doi.org/10.1016/0927-0256(96)00008-0

[16] Kresse, G. & Furthmüller, J. Efficient iterative schemes for *ab initio* total-energy calculations using a plane-wave basis set. *Phys. Rev. B* **54**, 11169–11186 (1996). https://doi.org/10.1103/PhysRevB.54.11169

[17] Blöchl, E. P. Projector augmented-wave method. *Phys. Rev. B* **50**, 17953–17979 (1994). https://doi.org/10.1103/PhysRevB.50.17953

[18] Kresse, G. & Joubert, D. From ultrasoft pseudopotentials to the projector augmented-wave method. *Phys. Rev. B* **59**, 1758–1775 (1999). https://doi.org/10.1103/PhysRevB.59.1758

[19] Perdew, J. P., Burke, K. & Ernzerhof, M. Generalized gradient approximation made simple. *Phys. Rev. Lett.* **77**, 3865 (1996). https://doi.org/10.1103/PhysRevLett.77.3865

[20] Ganose, A. M. *et al*. Efficient calculation of carrier scattering rates from first principles. *Nat. Commun.* **12**, 2222 (2021). https://doi.org/10.1038/s41467-021-22440-5

[21] Madsen, G. K. H. & Singh, D. J. BoltzTraP. A code for calculating band-structure dependent quantities. *Comput. Phys. Commun.* **175**, 67–71 (2006). https://doi.org/10.1016/j.cpc.2006.03.007

[22] Polyanskiy, M. N. Refractiveindex.info database of optical constants. *Sci. Data* **11**, 1–19 (2024). https://doi.org/10.1038/s41597-023-02898-2

[23] Riffe, D. M. Temperature dependence of silicon carrier effective masses with application to femtosecond reflectivity measurements. *J. Opt. Soc. Am. B* **19**, 1092–1100 (2002). https://doi.org/10.1364/JOSAB.19.001092

[24] Naik, G. V., Shalaev, V. M & Boltasseva, A. Alternative plasmonic materials: Beyond gold and silver. *Adv. Mater.* **25**, 3264–3294 (2013). https://doi.org/10.1002/adma.201205076

[25] Chen, Y. B & Zhang, Z. M. Heavily doped silicon complex gratings as wavelength-selective absorbing surfaces. *J. Phys. D* **41**, 095406 (2008). https://doi.org/10.1088/0022-3727/41/9/095406

[26] Faruque, O., Al Mahmud, R. & Sagor, R. H. Heavily doped silicon: A potential replacement of conventional plasmonic metals. *J. Semicond.* **42**, 062302 (2021). https://doi.org/10.1088/1674-4926/42/6/062302

[27] Chandra, H. *et al*. Open-source automated mapping four-point probe. *Materials* **10**, 110 (2017). https://doi.org/10.3390/ma10020110

[28] Schroder, D. K. *Semiconductor Material and Device Characterization*, *Third Edition.* (John Wiley & Sons, Inc., 2006) https://doi.org/10.1002/0471749095